Interior phase transformations and mass-radius relationships of silicon-carbon planets

Hugh F. Wilson

CSIRO Materials Science & Engineering, Parkville Victoria 3052 Australia

hugh.wilson@csiro.au

and

Burkhard Militzer

Department of Earth & Planetary Science and Department of Astronomy, University of California Berkeley, Berkeley, California

Received _____; accepted _____

ABSTRACT

Planets such as 55 Cancri e orbiting stars with a high carbon-to-oxygen ratio are considered to consist primarily of silicon and carbon, with successive layers of carbon, silicon carbide and iron. The behaviour of silicon-carbon materials at planetary interior pressures at the extreme pressures prevalent in planetary interiors, however, has not yet been sufficiently understood. In this work we use simulations based on density functional theory to determine high-pressure phase transitions in the silicon-carbon system, including the prediction of new stable compounds with Si_2C and SiC_2 stoichiometry at high pressures. We compute equations of state for these silicon-carbon compounds as a function of pressure, and hence derive interior structural models and mass-radius relationships for planets composed of silicon and carbon. Notably, we predict a substantially smaller radius for SiC planets than in previous models. We also compute a new equation of state for iron. We rederive interior models for 55 Cancri e and are able to place more stringent restrictions on its composition.

Subject headings:

1. Introduction

The chemical diversity of stars in the universe is expected to result in an even greater chemical diversity among the planets which they host. According to condensation models (Bond et al. 2010; Kuchner & Seager 2005), a key variable determining the chemical makeup of planets is the carbon-to-oxygen ratio of the disk. In stellar nebuae with carbon-oxygen ratios in excess of 0.8 (Bond et al. 2010), condensation models predict solid bodies within the ice line to consist primarily of silicon carbide and carbon rather than the silicate materials of our own solar system, leading to the formation of solid planets consisting of silicon, carbon and possibly iron with minimal oxygen (Bond et al. 2010). Recent work on carbon-based planets has been particularly motivated by the detection of planets in the 55 Cancri system, whose carbon-oxygen ratio is likely to be in excess of 0.8 although measurement of this quantity remains uncertain (Teske et al. 2013). In particular the planet 55 Cancri e, whose mass-radius relationship suggests it may be insufficiently dense for a silicate composition (Demory et al. 2011), has been modelled as consisting of layers of carbon, SiC and iron (Madhusudhan et al. 2012).

The accuracy of interior models of carbon-based planets has been hampered by a lack of experimental or theoretical data on the behaviour of silicon-carbon materials at high pressures. The best available equations of state for high-pressure silicon carbide are based on the extrapolation of experimental data (Aleksandrov et al. 1989; Seager et al. 2007). Although the high pressure phase diagram of carbon and equation of state of has been extensively studied up to extremely high pressures of 100 Mbar using ab-initio theory (Martinez-Canales et al. 2012), the phase diagram of silicon carbide and pure silicon have not been studied at multi-megabar pressures. Furthermore, as we shall show, the assumption that SiC remains the sole stable stoichiometry of the silicon-carbon binary system at extreme pressures is not justified, analogous to the anomalous stoichiometries

seen at high pressures in materials such as $MgSiO_3$ (Umemoto et al. 2006) and H_2O (Zhang et al. 2013; Pickard et al. 2013). In order to build accurate interior models of silicon-carbon rich planets and hence to determine expected mass-radius relationships for silicon-carbon planets as a function of composition, it is thus necessary to more accurately model the high-pressure behaviour of these materials.

In this work, we compute the high-pressure phase diagram and equations of state of the silicon-carbon binary system up to pressures of 40 Mbar. We use an *ab initio* random structure search algorithm to find relevant high-pressure phases of silicon, carbon, silicon carbide and Si_nC_m compounds of alternative stoichiometries. We predict new high-pressure phases of silicon carbide and silicon, and new stable high-pressure compounds with stoichiometry Si_2C and SiC_2. We compute equations of state for each relevant material and derive mass-radius relationships for silicon-carbon planets with interior pressures up to 40 Mbar. Our equation of state for SiC is twelve percent denser that used by Seager *et al*, leading to substantially smaller radii for silicon-carbon planets than had previously been suggested. We derive layered models for planets which take the novel Si_2C and SiC_2 phases into account In addition, we revise earlier equations of state for high-pressure iron. Our new results allow a refinement of the interior models of 55 Cancri e derived by Madhusudhan et al. (2012) which allow us to put stronger constraints on possible compositional models for this planet; in particular we eliminate possibilities of pure SiC or SiC-iron compositions.

2. Phase diagram of the silicon-carbon system

For pressures higher than 4 Mbar that cannot be reached with diamond anvil cell experiments, our understanding of planetary materials relies primarily on theoretical methods. In order to compute equations of state of silicon and carbon containing materials at high pressure, it is first necessary to know the phase diagram of the silicon-carbon

binary system including the onset of phase transitions and the stoichiometric relationships, requiring a search through the space of possible structures to find the ground-state phase and stoichiometry as a function of pressure. The Ab Initio Random Structural Search (AIRSS) algorithm (Pickard & Needs 2006) has emerged as a successful method for finding stable crystal structures of materials, particularly at high pressures, with an efficiency comparable to more algorithimically complex methods such as genetic algorithms. In the AIRSS methodology, randomly generated cell geometries are filled with randomly positioned atoms. Efficient geometry relaxation procedures are used to find the nearest local minimum. Although most randomly generated structures do not lead to the absolute ground state structure, it is found that a sufficiently large portion do so to allow the identification of ground state. Consistently and repeatedly finding a single structure to be lower in enthalpy than all competing structures may be considered to be reasonable evidence that it is the true lowest-enthalpy structure at that pressure. Although no optimisation scheme can be guaranteed to find the lowest-enthalpy structure, the past success of AIRSS (Pickard & Needs 2011) gives us reasonable confidence in its ability to produce ground state structures.

Here *ab initio* random structure searches were undertaken at 10, 20 and 40 Mbar. For each set of pressure and stoichiometry (C, Si, SiC and Si_mC_n structures detailed below), we begin by generating at least eight hundred random structures of between one and four stoichiometric units. All density functional theory theory (DFT) simulations in this paper used the VASP code (Kresse & Furthmüller 1996), pseudopotentials of the projector augmented wave type (Blöchl 1994) and the exchange-correlation functional of Perdew et al. (1996). The positions are initially optimised using a conjugate gradient algorithm until the difference between successive energies is less than 0.001 eV, using a plane wave cutoff of 500 eV and a grid of $4 \times 4 \times 4$ k-points to sample the Brillouin zone. Following the initial runs, the fifty structures lowest in enthalpy are subjected to a second, more accurate minimisation which uses a denser $12 \times 12 \times 12$ k-point grid and a 1200 eV cutoff

energy for the plane wave expansion. Finally, to obtain accurate enthalpy-pressure curves we recompute the stablest few structures using a 1200 eV cutoff and $32 \times 32 \times 32$ k-points, to ensure accurate and comparable enthalpies between structures with different cells. As a sole exception, a $24 \times 24 \times 24$ k-point grid was used for the SiC rocksalt structure due to memory constraints, however this should not have an appreciable effect on our results.

Table 1. Equation of state data including density and enthalpy per atom for silicon-carbon material phases.

Species	Structure	Pressure (Mbar)	Density (g/cc)	Enthalpy (eV/atom)
C	Diamond	10.0	6.9604	14.0268
C	BC8	20.0	9.0754	29.3157
C	sc	30.0	10.9662	41.9489
C	sc	40.0	12.1622	52.6657
SiC	Rocksalt	10.0	8.9794	23.8815
SiC	Rocksalt	20.0	11.4365	44.1922
SiC	Cmcm	30.0	13.8407	60.7266
SiC	Cmcm	40.0	15.4883	74.8858
Si	fcc	10.0	9.6443	36.6189
Si	fcc	20.0	12.3085	63.0787
Si	bcc	30.0	14.5602	84.8214
Si	bcc	40.0	16.2821	103.6850
Si_2C	I4/mcm	10.0	9.6143	28.4635
Si_2C	I4/mcm	20.0	12.2461	49.9598
Si_2C	I4/mcm	30.0	14.2369	67.7320
Si_2C	I4/mcm	40.0	15.9022	83.3526
SiC_2	Cmmm	10.0	8.7326	21.4377
SiC_2	Cmmm	20.0	11.1627	39.4868
SiC_2	Cmmm	30.0	12.9951	54.3792
SiC_2	Cmmm	40.0	14.5414	67.4479

Note. — Table 1 is published in its entirety in the electronic edition of the *Astrophysical Journal*. A portion is shown here for guidance regarding its form and content.

High-pressure phases of elemental carbon have been the study of a multiplicity of previous studies (Yin 1984; Grumbach & Martin 1996; Correa et al. 2008), and most recently an AIRSS study (Martinez-Canales et al. 2012) which predicted zero-temperature phases of carbon up to 100 Mbar. We find an identical progression of ground-state structures, shown in Figure 1. Our transition pressures match those of previous calculations, with carbon in the diamond phase transitioning to the BC8 phase at 10.0 Mbar and then to the simple cubic structure at 28.9 Mbar, compared to 9.9 and 29.0 Mbar in Martinez-Canales et al. (2012).

Pure silicon has been the study of fewer high-pressure theoretical studies. A transition from the hexagonal close packed (hcp) to the face-centered cubic (fcc) structure was predicted and experimentally confirmed to occur at 0.78 Mbar by Duclos *et al* (Duclos et al. 1987). Using AIRSS we confirm the fcc structure to remain the ground state structure at 10 and 20 Mbar. However, at 40 Mbar we find the body centered cubic (bcc) structure to be stabler. From a plot of enthalpy vs pressure (Figure 1) we find a transition from bcc to fcc at 27 MBar.

Although silicon carbide at lower pressures exhibits a complex phase diagram, the high-pressure phase diagram is relatively simple. At 10.5 kBar, silicon carbide is known experimentally to transform into the rocksalt phase (Sekine & Kobayashi 1997). No other structure has been predicted at higher pressures. Our calculations find the rocksalt phase to remain stable at pressures as high as 10 and 20 Mbar. At 40 Mbar, however, we find a new SiC structure with *Cmcm* symmetry to be the stablest geometry. This structure is found to be structurally identical to the B33 structure of CrB, and is a layered structure in which each C or Si atom has five equally near neighbours of the opposite species within one layer unit, and two slightly further neighbours of the opposite species in the next layer. Structural parameters of the *Cmcm* SiC structure are given in online supplementary

material. The transition from the rocksalt to the *Cmcm* structure is found to occur at 27 Mbar.

We now turn our attention to the search for silicon-carbon structures with alternative stoichiometries. Here we restrict our attention to structures with simple integer ratios of atomic species – C:Si = 1:2, 1:3, 1:4, 2:3, 2:1, 3:1, 4:1 and 3:2. The space of compounds with each of these stoichiometries up to 4 functional units per cell was searched at 40 Mbar, and the enthalpy of the stablest compounds at each stoichiometry plotted as a function of elemental ratios in a convex hull diagram as seen in Figure 2. The convex hull diagram depicts the stability of material phases as a function of their chemical composition. If a point lies below the line joining two adjacent compositions then this structure is stable relative to an (unmixed) combination of the adjacent phases. At 40 Mbar it is found that two new stoichiometries have become stable relative to the combination of other compounds: SiC_2 (stabler than SiC + C) and Si_2C (stabler than SiC + Si).

The SiC_2 structure found at 40 Mbar is a structure with *Cmmm* symmetry. The *Cmmm* structure consists of alternating rows of silicon atoms, which are bonded to four silicon atoms in a planar configuration, and a second class of carbon atoms which are bonded to six silicon atoms. We are not aware of any other compound displaying this crystal structure. Structural parameters of the *Cmmm* structure are given in online supplementary material. Subsequent AIRSS searches at 20 and 10 Mbar found this structure to remain the ground-state stoichiometry at these lower pressures.

For Si_2C, a structure with *I4/mcm* symmetry was found to be the ground state at 40 Mbar. Examination of this structure reveals it to be identical to the C16 structure of Al_2Cu. In this structure, carbon atoms form close-packed linear chains with each carbon atom equidistantly spaced from eight Si atoms. Structural parameters of this structure are given in Table **??**. Similar to the SiC_2 case, AIRSS searches at 20 and 10 Mbar found this

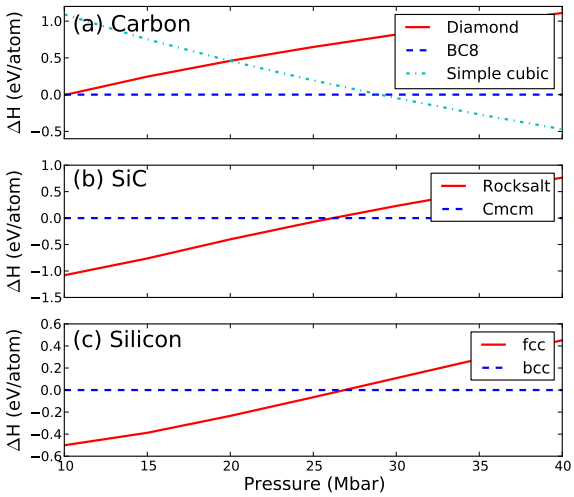

Fig. 1.— Pressure vs enthalpy plot for the examined structures at zero temperature for (a) carbon, (b) SiC and (c) silicon. Only structures which represent the thermodynamic ground state at some pressure between 10 and 40 Mbar are shown.

structure to remain the ground-state stoichiometry at these lower pressures.

Next, we computed equations of state of each for the SiC_2 and Si_2C structures the formation energy relative to SiC + Si or SiC + C. Figure 3 shows the enthalpy of the Si_2C and SiC_2 phases relative to separate phases of SiC and C/Si. It is found that SiC + Si will form the *I4/mcm* Si_2C phase at 13 Mbar, with the formation enthalpy continuing to increase with pressure. The *Cmmm* SiC_2 structure becomes stable at a higher pressure of 23 Mbar relative to SiC + C. The phase transition to the simple cubic structure of carbon, however, results in the formation enthalpy of SiC_2 decreasing above 29 Mbar. Although SiC_2 remains stable relative to SiC + C at 40 Mbar, the highest pressure studied here, a transition back to SiC + C stability is possible at higher pressures but lies beyond the scope of this work.

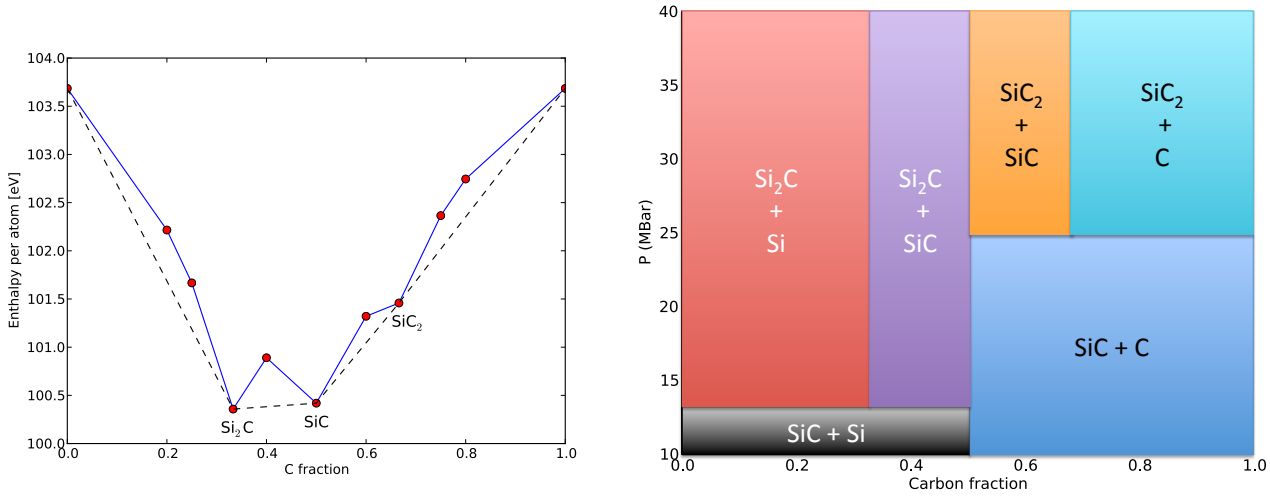

Fig. 2.— (a) Convex hull diagram depicting enthalpy versus carbon fraction for compounds in the silicon carbon binary system at 40 Mbar. (b) Phase diagram showing the stable mixture of phases formed for silicon-carbon stoichiometries as a function of composition and pressure from 10 to 40 Mbar.

3. Equation of State Results and Mass-Radius Relationship

Having now established the phase diagram of the silicon-carbon system, we now compute volume and enthalpy results as a function of pressure. Since our goal is to determine mass-radius relationships on a planetary scale, we ignore for the purpose of this calculation low-pressure phases such as graphite and the many phases of SiC existing below 10 kbar, which affect only the first few tens or hundreds of kilometres of the planet. A representative sample of the equation of state data is shown in Table I, with the full equation of state data, at a larger number of pressures, available in machine-readable format in online supplementary material.

In Fig. 4, we compare our DFT-based SiC equation of state calculations with two equations of state that were constructed for SiC previously. First we show a Birch-Murnaghan fit that was constructed from the high-pressure diamond anvil cell

experiments by (Aleksandrov et al. 1989). The density of SiC was determined with x-ray diffraction measurements up to a pressure of 0.425 Mbar. Results were fit to a third order Birch-Murnaghan equation (Birch 1947). Even though this equation was constructed to describe the compression of materials, significant uncertainties are introduced when one extrapolates this EOS fit by two orders in pressure. It is therefore not too surprising that our DFT calculations predict densities for SiC that are between 20 and 35% higher. (Seager et al. 2007) combined the experimental results by Aleksandrov *el. al.* with the predictions from the Thomas-Fermi-Dirac theory (Salpeter & Zapolsky 1967) in order to construct a modified polytrope equation of state for SiC for the purpose of planetary interior modeling, which was later also used by Madhusudhan et al. (2012). The densities derived from the modified polytrope equation of state are approximately 12% lower than we obtained with DFT calculations. This correction directly implies that the radii of SiC planets have been significantly overestimated previously (Seager et al. 2007; Madhusudhan et al. 2012). Since DFT has been validated for a wide range of materials and thermodynamic conditions (Tuckermann 2002; Kirchner et al. 2012; Parrinello 1997) and the Thomas-Fermi-Dirac theory only becomes valid at ultra-high pressures where chemical bonds can no longer exist, we consider our DFT results significantly more reliable in the megabar regime under consideration.

Following Seager et al. (2007), we solve the equations of hydrostatic equilibrium and mass conservation to derive the mass-radius relationship of different planets,

$$\frac{dP}{dr} = -\frac{Gm\rho}{r^2}, \tag{1}$$

$$\frac{dm}{dr} = 4\pi r^2 \rho. \tag{2}$$

We start the integration in the planet's center with $r = 0$, $m = 0$, and a central

pressure, $P = P_c$ and then integrate outwards until the pressure decreases to zero. $m(r)$ labels the mass that is enclosed in radius r. The second equations describes how $m(r)$ changes when a new mass shell is added. The first equation characterizes the change in pressure that balances the difference in gravitational potential that an additional layer introduces. For efficiency reasons, we solve these equations with a fourth order Runge-Kutta method using a fixed step size of $dr = 50\,\mathrm{km}$. Alternatively a simple Euler integration with $dr = 1\,\mathrm{km}$ may also be used. The equation of state only enters through $\rho = \rho(P)$. We assume that temperature effects are small (Seager et al. 2007). For each material's phase, we construct a separate spline function, $\rho = \rho(P)$, to interpolate our DFT results. When a phase transition occurs at a certain pressure, we switch discontinuously from one spline function to the next.

We integrated the equations 1 and 2 for pure SiC planets to learn how differences in the equation of state affect the mass-radius relationship. Figure 4 shows that our DFT results imply that SiC planets are approximately 5% smaller than predicted by Seager et al. (2007) and Madhusudhan et al. (2012). Because of this correction, it is no longer valid to model 55 Cancri e as a pure SiC planet, which was one possible scenario that was recently proposed by Madhusudhan et al. (2012) among other interior models. Our DFT results instead predict 55 Cancri e to have another light outer layer in addition to the SiC core. A likely candidate would be a carbon layer.

Following Madhusudhan et al. (2012), we constructed a suite of ternary interior models with an iron core, a SiC mantle and an outer carbon layer. The central pressure, P_c, and the pressures where we switch from iron to SiC, P_1, and from SiC to carbon, P_2, are free parameters. We constructed a fine 3D grid ranging from $6.5 \leq P_c \leq 24.5\,\mathrm{Mbar}$ and $0 \leq P_1/P_c \leq 1$ and $0 \leq P_2/P_1 \leq 1$. We selected models where the sum of the χ^2 deviations in mass and radius from the observed values were less than 2. We adopted a radius value

of $2.173^{+0.097}_{-0.098} R_E$ that combined Spitzer and MOST observations (Gillon et al. 2012) rather than constructing interior models for each radius measurement separately. A mass of $M = 8.39 \pm 0.38 M_E$ (Endl et al. 2012) was assumed. All valid models are summarized in the compositional diagram in Fig. 5. When we performed this analysis with a modified polytrope EOS for SiC, our results are consistent those by Madhusudhan et al. (2012) and a planet of pure SiC would be consistent with observations. However, when we switch to using our more accurate DFT EOS for SiC, maximum SiC fraction drops to only 52%. Because we predict SiC to be a denser material, a thick outer carbon layer must compensate for this change.

In Fig. 5, we compare the iron and SiC mass fractions from our Fe-SiC-C models that match the observed mass and radius. In the inset we display the same information in a conventional ternary composition diagram where each corner corresponds to a planet of one material only. When we compared the effects of using our DFT equation of state for SiC with the modified polytrope EOS from Seager et al. (2007), all other model parameters were kept constant. Both equations of state consistently predict that 55 Cancri e can only contain up to 18% iron. This limit appears to be insensitive to changes in the SiC and Fe equations of state because the density of iron is so much higher than that of the other materials. Based on our DFT results, we predict 55 Cancri e to be a carbon rich planet with a carbon fraction of 48% or more. All permitted models fall into a triangle in composition space that is spanned by three limiting cases: a) pure carbon planet, b) an iron-free SiC-C planet with 48% carbon, and c) an SiC-free iron-carbon planet with 82% carbon. It is not possible to resolve this degeneracy with the existing constraints on mass and radius. In principle, additional information we be obtained from *in situ* simulations (Bond et al. 2010).

4. Interior Structure of Si-C Planets

In this section, we explore how the formation of the novel compounds, SiC_2 and Si_2C, will affect in the interior structure of Si-C planets. From our DFT simulations, we derived the compositional phase diagram in Fig. 3. This diagram describes which minerals would form from a Si-C mixture at a certain pressure. For example a carbon-rich Si-C mixture would split into SiC and carbon for pressures up to 25 Mbar. For higher pressures, this mixture would split into SiC_2 and SiC or, for carbon fractions larger than 67%, would form SiC_2 and carbon. For silicon-rich assemblages, a similar change is triggered by the formation of Si_2C at 13.6 Mbar.

First we will discuss the formation of a carbon-rich planet with carbon atom fraction of 95%. We make the assumption of homogeneous accretion of SiC and carbon in fixed proportions. Materials in the planetary interior differentiate and form separate layers that are sorted by density. Each layer is assumed to be homogenous but have distinct chemical composition and be fully convective. As we know from Earth, phase transitions will not inhibit convection unless they are associated with chemical heterogenities.

For an accreting carbon-rich planet, these assumptions and the phase diagram in Fig. 3 imply the formation of a two-layer planet with a SiC core and carbon mantle until the planet exceeds a critical size. For a carbon fraction of 95%, this critical size corresponds to a planet with a radius of $2.886R_E$ and a mass of $24.92M_E$ as illustrated in Fig. 6 a. The SiC core would be comprised of only $2.77M_E$ and have a radius of $1.04R_E$. If the pressure at the core-mantle boundary exceeds 25 Mbar, SiC_2 will form from SiC and carbon. Since SiC_2 has an intermediate density, this new layer will form in between the SiC core and carbon layer. If additional SiC-C material is accreted onto the surface of the planet, the increased gravitational force will temporarily increase the pressure at the SiC_2-C boundary beyond 25 Mbar. When the sinking SiC material arrives to the bottom of the carbon layer, it will

react with the carbon present to form additional SiC_2. Assuming plenty of SiC is available, this implies the existance a feedback mechanism that stabilizes the pressure at the SiC_2-C boundary at 25 Mbar during accretion.

However, determining whether sufficient SiC is available at SiC_2-C boundary is not straightforward. If one grows the planet assuming a constant total composition and that the SiC_2-C boundary remains at the critical pressure of 25 Mbar, then some reactant SiC material has to come from the SiC core. Assuming the core provides sufficent SiC, the planet will assume the state of *chemical equilibrium* shown in Fig. 6 b. As the planet mass increases from 27.68 to 29.00 M_E during accretion, the SiC core would shrink from 2.77 to only 1.32 M_E in such a model. This would require a significant amount of gravitational energy and it is not obvious which mechanism could provide that. However, planetary interiors are complex and the equilibrium model is certainly one that needs to be considered. The scenario of a shrinking SiC core would share some similarities with the core erosion that has been proposed to occur in giant planets (Guillot et al. 2004; Wilson & Militzer 2012b,a; Wahl et al. 2013).

In the absence of any obvious energy source that would be needed to shrink the SiC and bring the whole planet into chemical equilibrium, we also wish to discuss an alternative *dynamic scenario*, where no mass is removed from the SiC core. We assume the SiC core would grow up to the maximum size that is reach when the pressure at the SiC_2-C boundary attains 25 Mbar. From that point on, the SiC_2 layer would only grows from newly accreted SiC material that sinks through the carbon layer. As the planet mass increases from 27.68 to 29.00 M_E, SiC core would only be more compressed and its radius would shrink from 1.04 to 1.02 R_E. A comparatively thin SiC_2 layer would form that comprises only 0.20 M_E compared to 2.37 M_E in the equilibrium scenario. The SiC_2 layer would be starved for SiC and the pressure at the SiC_2-C boundary would reach 26.2 Mbar (Fig. 6 c). This

exceeds the 25 Mbar needed for SiC_2 formation but there is insufficient SiC available. This condition is also consistent with the phase diagram in Fig. 3.

For a fixed planet mass and carbon fraction, the deviations in the predicted radii between the equilibrium and the dynamic scenario are very small. For a planet of 29 M_E, we obtained 2.892 and 2.895 R_E, respectively. We conclude either model can be use to compare with observations in the future.

For a silicon-rich planet with a carbon atom fraction of 45%, the differences between the equilibrium and the dynamic scenario area bit more pronounced because the Si_2C forms already 13.6 Mbar. A planet may accrete up to 11.62 M_E and reach a radius of 2.091 R_E before the Si_2C layer forms (Fig. 7 a). According to the equilibrium model, the SiC core would then completely absorbed into the growing Si_2C layer (Fig. 7 b) as the planet reaches a total mass of 16.15 M_E. An amount of 4.84 M_E of Si_2C would be formed according to the equilibrium picture, while in the dynamic scenario one would predict an intermediate Si_2C layer of only 1.36 M_E to form. Fig. 7 shows that the predicted planet radii are again very similar.

In Fig. 8, we summarize the mass-radius relationships of different types of planets. For this purpose, we also revisited the accuracy of the iron EOS used in Seager et al. (2007) by performing DFT calculations of the relevant *bcc* and *hcp* phases. We identified a modest correction. At 10 and 40 Mbar, we predict densities 2.2% and 4.7% higher. The predicted radii of pure iron planets with 5 and 10 Earth masses would shrink by 1% and 2% respectively.

We added the different types of Si-C planets to Fig. 8. As expected, Si-C planets with 45% and 95% carbon closely track results of the pure SiC and pure carbon planet, respectively. The formation of intermediate Si_2C and SiC_2 layers does not affect the mass-radius relationship significantly. More surprising is that radii of pure SiC planets are

very similar to those of rocky planets made of 100% silicates. Our revision of the SiC EOS put this material much closer to silicate rocks. Therefore, SiC cannot serve a low-density material to explain the interior structure when observations suggest a radius larger than that of pure silicate planets.

5. Conclusions

We have conducted extensive simulations of the phase diagram and equation of state of the silicon-carbon system at pressures up to 40 Mbar. Using ab-initio random structure search methods, we predicted a new phase of silicon carbide and a bcc to fcc transition in silicon. In addition, we find two phases, SiC_2 and Si_2C which are formed at high pressures for carbon-rich or silicon-rich stoichiometries respectively. Our newly calculated equation of state for silicon carbide is approximately five percent denser at high pressures than the extrapolated equation of state used in previous works, leading to a significant downwards revision of predicted mass-radius relationships for SiC-C planets and eliminating the possibility of a 55 Cancri e model made of pure SiC. We also present a revised equation of state for iron.

At present, 55 Cancri e remains the sole identified candidate for a silicon-carbon dominated exoplanet, however its C/O ratio is not yet well enough constrained to eliminate the possibility that the planet may be silicate-dominated after all. Future work to identify and characterise additional carbon planet candidates may be able to resolve the question of the existence and composition of carbon-based planets.

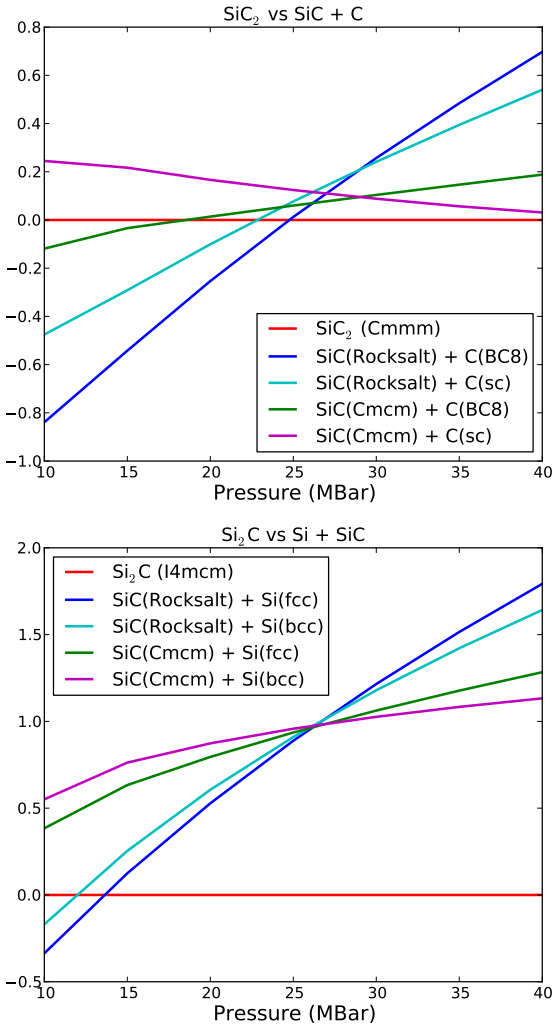

Fig. 3.— (a) Pressure vs enthalpy graph for the examined Si_2C and Si_2C structures. (b) Phase diagram of composition versus pressure for the silicon carbon binary system at pressures from 10 to 40 Mbar.

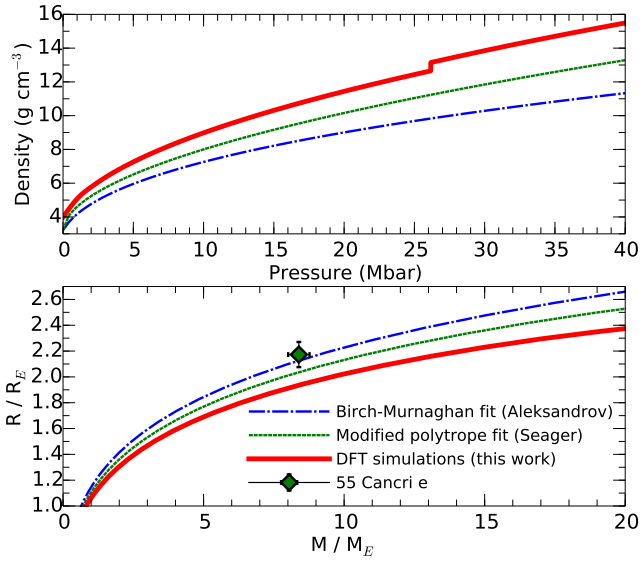

Fig. 4.— The upper panel compares the density of SiC as function of pressure predicted from our DFT calculations with the Birch-Murnaghan fit to the experimental data (Aleksandrov et al. 1989) and modified polytrope EOS by Seager et al. (2007). The discontinuity of DFT curve marks the phase transition from the rocksalt to the *Cmcm* structure. Since our DFT calculations predict SiC to be more dense at megabar pressures, we predict the radii of SiC planets to be significantly smaller, which is illustrated in the lower panel. Thus, 55 Cancri e can no longer be composed purely of SiC. A ligher outer layer, e.g. made of carbon, is needed to explain the oberved mass and radius.

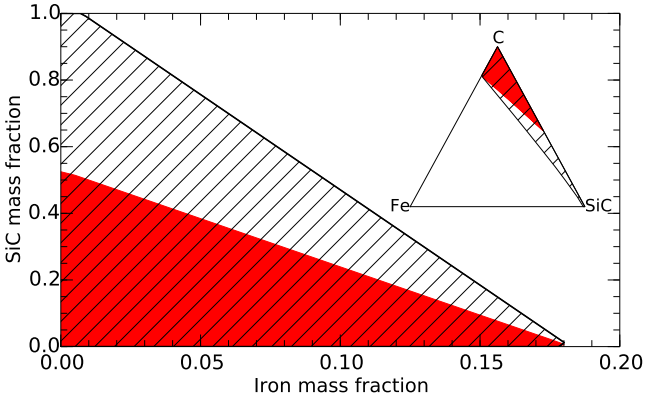

Fig. 5.— SiC vs. iron mass fraction for three-layer iron-SiC-C planet models that were constructed to match the observed mass and radius of 55 Cancri e, $M = 8.39 \pm 0.38 M_E$ and $2.173^{+0.097}_{-0.098} R_E$. The hatched area shows valid models based on a modified polytrope EOS of SiC (Seager et al. 2007). Using the our DFT SiC EOS, the permitted SiC fraction shrinks significantly (red filled area). The inset shows the same information in an conventional ternary compositional diagram where each corner corresponds to a planet made of only one material. The DFT results imply that 55 Cancri e is composed of 48% carbon or more.

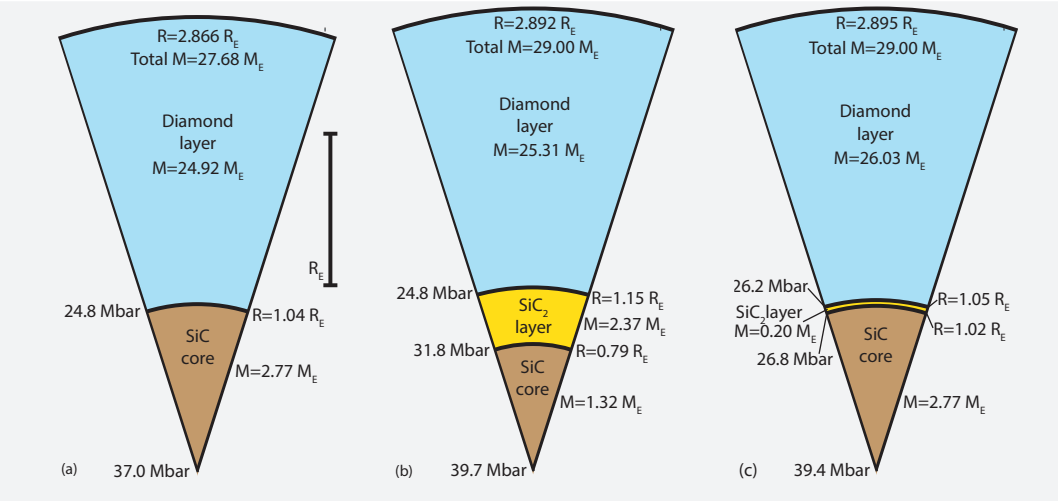

Fig. 6.— Interior models for Si-C planets with carbon fraction of 95%. The left panel illustrates the largest size such a planet can reach before an intermediate SiC_2 layer forms. The middle panel shows a planet in chemical equilibrium with such a layer. The right planet displays an alternative, dynamic interior model for the same total mass where the SiC core was not permitted to be absorbed into the forming SiC_2 layer.

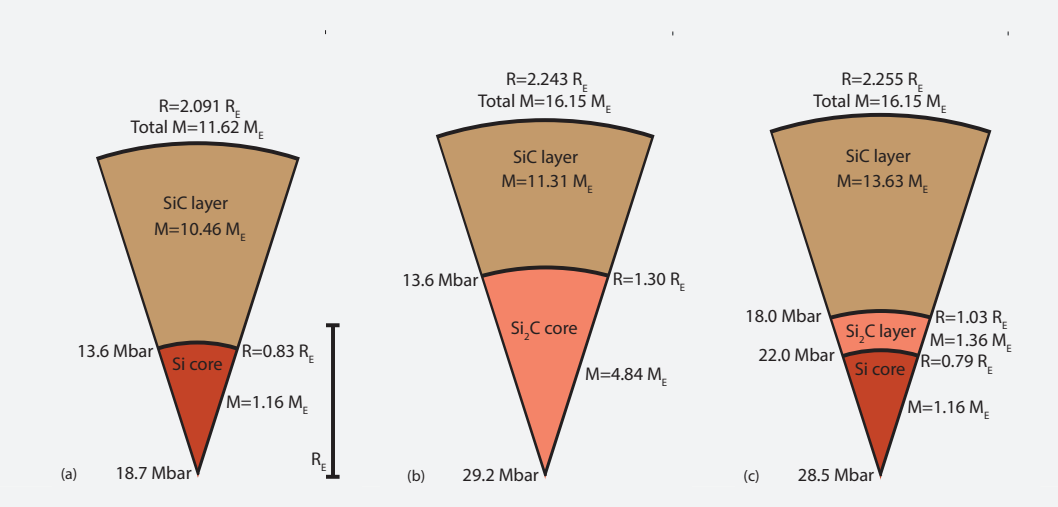

Fig. 7.— Interior models for Si-C planets with carbon fraction of 45%. Similar to Fig. 6, the left panel shows the largest possible planet without an intermediate Si_2C layer. The middle panel displays a planet in chemical equilibrium where the SiC core has been absorbed completely into Si_2C layer. with such a layer. The right planet shows an alternative, dynamic interior model where SiC core was not permitted to shrink.

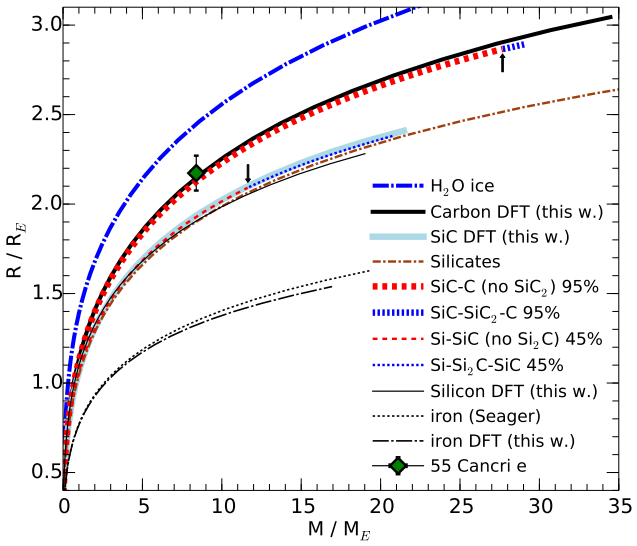

Fig. 8.— Mass-radius relationship for different types of planets in Earth units. The arrows indicate the minimum mass that is required for carbon and silicon-rich planets to form intermediate layers of SiC_2 and Si_2C, respectively. The mass percentage of carbon is indicated in the caption when appropriate.

REFERENCES

Aleksandrov, I. V., Goncharov, A. F., Stishov, S. M., & Yakovenko, E. V. 1989, J. Exp. Theor. Phys., 50, 127

Birch, F. 1947, Phys. Rev., 71, 809

Blöchl, P. E. 1994, Phys. Rev. B, 50, 17953

Bond, J. C., O'Brien, D. P., & Lauretta, D. S. 2010, Astrophys. J., 715, 1050

Correa, A. A., Benedict, L. X., Young, D. A., Schwegler, E., & Bonev, S. A. 2008, Phys. Rev. B, 78, 024101

Demory, B.-O., Gillon, M., Deming, D., et al. 2011, Astron. Astrophys., 533

Duclos, S. J., Vohra, Y. K., & Ruoff, A. L. 1987, Phys. Rev. Lett., 58, 775

Endl, M., Robertson, P., Cochran, W. D., et al. 2012, 759, 1

Gillon, M., Demory, B.-O., Benneke, B., et al. 2012, Astron. Astrophys., 539

Grumbach, M. P., & Martin, R. M. 1996, Phys. Rev. B, 54, 15730

Guillot, T., Stevenson, D. J., Hubbard, W. B., & Saumon, D. 2004, 35–57

Kirchner, B., di Dio, P. J., & Hutter, J., eds. 2012, Topics in Current Chemistry, Vol. 307, Real-World Predictions from Ab Initio Molecular Dynamics Simulations (Springer Berlin), 109

Kresse, G., & Furthmüller, J. 1996, Phys. Rev. B, 54, 11169

Kuchner, M. J., & Seager, S. 2005, arXiv

Madhusudhan, N., Lee, K. K. M., & Mousis, O. 2012, ApJ Lett, 759

Martinez-Canales, M., Pickard, C. J., & Needs, R. J. 2012, Phys. Rev. Lett., 108, 045704

Parrinello, M. 1997, Solid State Comm., 102, 107

Perdew, J. P., Burke, K., & Ernzerhof, M. 1996, Phys. Rev. Lett., 77, 3865

Pickard, C. J., Martinez-Canales, M., & Needs, R. J. 2013, Phys. Rev. Lett., 110, 245701

Pickard, C. J., & Needs, R. J. 2006, Phys. Rev. Lett., 97, 045504

—. 2011, J. Phys. Cond. Mat., 23, 053201

Salpeter, E. E., & Zapolsky, H. S. 1967, Phys. Rev., 158

Seager, S., Kuchner, M., Hier-Majumder, C. A., & Militzer, B. 2007, Astrophys. J., 669, 1279

Sekine, T., & Kobayashi, T. 1997, Phys. Rev. B, 55, 8034

Teske, J. K., Cunha, K., Schuler, S. C., Griffith, C. A., & Smith, V. V. 2013, Astrophys. J., 778, 132

Tuckermann, M. E. 2002, J. Phs. Cond. Matter, 14, R1297

Umemoto, K., Wentzcovitch, R. M., & Allen, P. B. 2006, Science, 311, 983

Wahl, S. M., Wilson, H. F., & Militzer, B. 2013, Astrophys. J., 773, 95

Wilson, H. F., & Militzer, B. 2012a, Phys. Rev. Lett., 109, 111011

—. 2012b, Astrophys. J., 745, 54

Yin, M. T. 1984, Phys. Rev. B, 30, 1773

Zhang, S., Wilson, H. F., Driver, K. P., & Militzer, B. 2013, Phys. Rev. B, 87, 024112